BN-Substituted Coronene Diimide Donor-Acceptor-Donor Triads: Photophysical, (Spectro)-Electrochemical Studies and Lewis Behavior

Jonas Hoffmann, [a,b,c] Denis Jacquemin, [d] Muriel Hissler [*c] and Anne Staubitz [*a,b]

Boron/nitrogen substituted polyaromatic hydrocarbons (**PAH**s) are unique materials, with similar molecular structures as their carbon/carbon analogs, but different electronic properties. We report how these may be tuned by substitution at the B and/or N atoms: The BN-PAH analogues we investigated are BN-substituted coronene diimide (**BNCDI**) acceptors, combined with electron-rich (hetero)arene substituents (donors) on the boron atoms at either side of the **BNCDI**, resulting in donor-acceptor-donor (**D-A-D**) triads. In comparison to the all-carbon coronene diimide, the implementation of two BN units led to a bathochromic shift of absorption/emission (44 nm) and luminescence quantum yields close to unity. The uniqueness of the BN-based **D-A-D** motif became clear as the substitution effect of the (hetero)arene substituents was investigated. The strong electron-donating triphenylamine motif had a minor influence on the absorption behavior but showed strongly solvent-dependent luminescence properties. This could be attributed to an intramolecular photoinduced electron transfer (**PeT**) process which was supported by a Rehm-Weller analysis and density functional theory computations. This process was not observed for the other substituents. Moreover, we probed the influence of the aryl substituent on the B-N bond itself by using (spectro)electrochemistry and analyzed the Lewis behavior of the BN unit. The species that formed showed strong absorptions across the whole UV/Vis/NIR region.

Introduction

Polycyclic aromatic hydrocarbons (PAHs) show outstanding electronic and optoelectronic properties and have potential applications in organic electronics.[1-6] Due to the tunability of the gap between the highest occupied molecular orbital (HOMO) and the lowest unoccupied molecular orbital (LUMO), their high conductivity and superior thermal stability, PAHs are ideal materials for organic solar cells (OSC), organic field-effect transistors (OFET), and organic light-emitting devices (OLED).[7-9] Among all PAH-based π-conjugated materials, rylene (naphthalene/perylene/coronene) diimide dyes have been most intensely studied because of their excellent (photo)chemical and thermal stability, high absorption coefficients, high fluorescence quantum yield, and acceptor properties.[10-12] As an example, the highest n-channel mobility (8.50 $cm^2 V^{-1} s^{-1}$) in an air-stable OFET is based on a naphthalene diimide copolymer.[13] The incorporation of single electron-rich heteroatoms (O,[14] S,[15-17] N[18, 19]) has already been shown to be a promising method for controlling the optical and electronic properties of these acceptor materials. A relatively new strategy for influencing these properties takes the opposite approach: The formal replacement of two carbon atoms by a combination of a nitrogen and a boron atom introduces both an electron-rich and electron-deficient atom. In this way, the number of valence electrons is unchanged (BN/CC isosterism),[20-23] the geometry of the conjugated π-system largely undisturbed, but the electron distribution is radically different.[4, 24-26] There is now a good variety of synthetic methods for embedding BN units in PAHs. They fall into one of three types of reaction: First, with the carbon skeleton fully in place, and an aniline function in an *ortho*-position, an amino-borane can be formed using an $RBCl_2$ species, which in turn can undergo an electrophilic arene borylation to an adjacent ring, thus closing the heterocycle.[27-30] The second method is based on transition metal-catalyzed cycloisomerization of ethynyl groups after the BN-bond has been already formed using platinium[31-33] or gold catalyst.[34] A third, less common method to access BN-PAHs is the use of ring-closing metathesis reactions,[35, 36] which originated from the synthesis of substituted 1,2-azaborines.[37] However, most of the recently synthesized BN-PAHs represent BN-analogs to prominent p-type organic materials, e.g. pyrene,[38, 39] perylene[34] or acenes.[33, 40] The implementation of BN units into structures that are already inherently electron-deficient, such as BN-substituted perylene diimide (**Ph-BNPDI**),[41] remains rare so far.

Carbon-based Donor (D) and acceptor (A) substituted π-conjugated compounds have been widely used for organic electronics,[42, 43] two-photon absorption,[44] and non-linear

[a] *University of Bremen, Institute for Analytical and Organic Chemistry, Leobener Straße 7, D-28359 Bremen, Germany. Email: staubitz@uni-bremen.de.*
[b] *University of Bremen, MAPEX Center for Materials and Processes, Bibliothekstraße 1, D-28359 Bremen, Germany.*
[c] *ISCR, Institut des Sciences Chimiques de Rennes, UMR 6226, CNRS-Université de Rennes 1, Campus de Beaulieu, F-35042 Rennes Cedex, France.*
[d] *Université de Nantes, CNRS, CEISAM UMR 6230, F-44000 Nantes, France*
Electronic Supplementary Information (ESI) available: Experimental conditions, full characterizations (^{1}H NMR, $^{11}B\{^1H\}$ NMR and $^{13}C\{^1H\}$ NMR spectra, HRMS, FTIR of all new compounds), UV-Vis, fluorescence and interaction with solvents and Lewis base/acids as well as computational details. See DOI: 10.1039/x0xx00000x

optics.[45] Molecular designs yielding push-pull **D-A** dyads and symmetric **D-A-D** triads are of special interest since they can serve as active material in ambipolar charge transfer semiconductors[46] and solar cells.[47, 48] Furthermore, **D-A** dyads

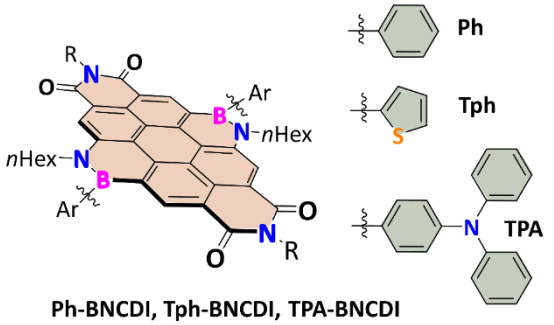


Fig. 1 Overview of aryl-substituted **BNCDI**s in which the imide substituent was either cyclohexyl (Cy), 2,6-di(*iso*propyl)phenyl (Dip) or *n*hexyl (*n*Hex).

absorptions due to their intramolecular charge transfer (**ICT**) character.[49] For example, electron-accepting perylene diimides (**PDI**s) that were symmetrically flanked with electron-donating groups, exhibited significantly smaller HOMO/LUMO gaps, due to the destabilization of the HOMO level by the donor, resulting in bathochromically shifted and broad absorption bands.[50-53] The careful design of such systems, and especially of the balance between the emissive **ICT** and non-emissive processes, are fundamental for application as luminophores. In particular, it is known that combinations of electron-accepting rylene diimides with electron-donating triphenylamine groups can induce both twisted intramolecular charge transfer (**TICT**)[51, 52, 54] and photoinduced electron transfer (**PeT**)[55] processes which both quench the luminescence. The investigation of complex BN-PAH structures being still in its infancy, such molecular designs have not been prepared for any BN-substituted PAHs yet. Synthetically, **D-A-D** triads may be generated in a symmetrical di-BN-substituted PAH by the introduction of electron-donating substituents (**D**) to the two BN units which are incorporated and are part of the acceptor (**A**) system.

In this work, we report a series of **D-A-D** triads, in which dually BN-substituted coronene diimides (**BNCDI**) were combined with mildly, medium, and strongly electron-donating groups attached to the boron atoms allowing tuning of the optoelectronic properties of the core according to the donor strength of the substituents. It emerged that such an electronic tuning resulted in minor changes of photophysical response in the ground-state but had a strong impact on the excited state. Furthermore, the interactions with Lewis bases, acids, and weakly coordinating solvents influence also substantially the optoelectronic properties. To rationalize our observation, the photophysical phenomena were thoroughly investigated by absorption and luminescence spectroscopy as well as (spectro)electrochemistry.

Results and Discussion

Using a well-established electrophilic borylation reaction of arylamines,[56] we synthesized seven novel BN-substituted coronene diimides (**BNCDI**s) with varying aryl groups (phenyl, 2-thienyl, 4-triphenylamine) at the boron atom and different substituents (*n*hexyl, cyclohexyl, 2,6-di*iso*proyplphenyl) at the imide position (Fig. 1; For synthetic details see the ESI). The chemical structures of all **BNCDI**s were confirmed by ^{1}H, ^{11}B{^{1}H} and ^{13}C{^{1}H} NMR spectroscopy, FTIR analysis, and high-resolution mass spectrometry (HRMS). Because PAHs are often processed by evaporation processes, we probed the thermal stability of these compounds by thermogravimetric analysis (TGA). All **BNCDI**s showed high thermal stabilities (T_{95} >350 °C), which were essentially unaffected by the respective aryl-substituents at the boron atom or the imide nitrogen atom (Table 1, TGA curves are found in Fig. S84 in the ESI).

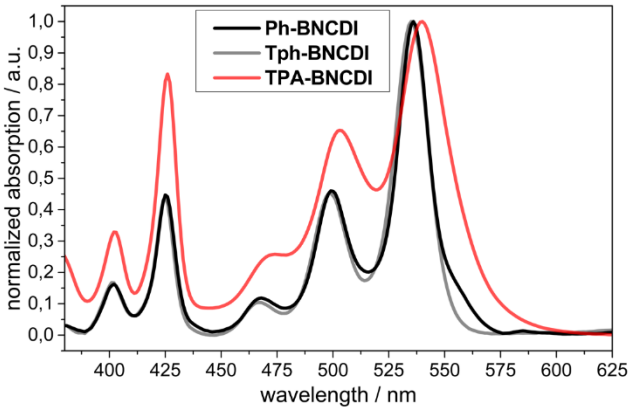


Fig. 2 Absorption spectra of **Ph-BNCDI**, **Tph-BNCDI** and **TPA-BNCDI** in DCM (10^{-5} M).

Table 1 Overview of the optical and thermal properties of the here discussed **BNCDI**s.

compound	λ_{abs} [a] / nm	Lg(ε)[a]	E_{opt} /eV[b]	λ_{lum} [a] / nm	$\Delta\nu_{stokes}$ [a] /cm^{-1}	Φ_{lum} [c]	T_{95} [d] / °C
Ph-BNCDI	536	4.80	2.30	544	285	0.95	390
Tph-BNCDI	535	4.74	2.24	544	310	0.95	396
TPA-BNCDI	540	4.68	2.19	581	1307	< 0.01	359

[a] Measured in DCM solutions (10^{-5}-10^{-6} M) [b] Calculated from the offset wavelength derived from the lowest energy absorption band. [c] Referenced externally against fluorescein in 0.1 M NaOH. [d] TGA measurement: The temperature at which 95% of the mass was still present at a heating rate of 10 K/min and nitrogen flow of 20 mL/min.

Optical Properties

Comparison of BN vs CC in perylene/coronene diimides

The photophysical characteristics of the **BNCDI**s were determined using UV/Vis absorption and photoluminescence spectroscopy. All **BNCDI**s showed a first intense absorption band with vibronic fine structures in the higher energy region (380-440 nm) and a second absorption band with two vibronic peaks in a lower energy region (450 -580 nm) along with high ε (Fig. 2, Table 1). Since the imide substituents are electronically decoupled from the coronene core,[57] the substitution of the imide position did not influence the spectra and we focus solely on the cyclohexyl motif below (for the additional data for the 2,6-di*iso*proyplphenyl- substituted molecules see the ESI).

The absorption maxima of **BNCDI**s were between 535 nm and 541 nm and thus they were red-shifted compared to their CC-isosteres **CDI** (λ_{abs} =494 nm),[57] **PDI** (λ_{abs} = 525 nm),[58] and previously reported BN-monosubstituted **Ph-BNPDI** (λ_{abs} = 529 nm).[41] The strongly bathochromic shifted absorption of the **BNCDI**s in comparison to the **CDI** is remarkable. The analysis of the luminescence in DCM solutions showed that substitution with phenyl/thienyl groups in

Ph/Tph-BNCDIs gave compounds emitting green light with quantum yields close to

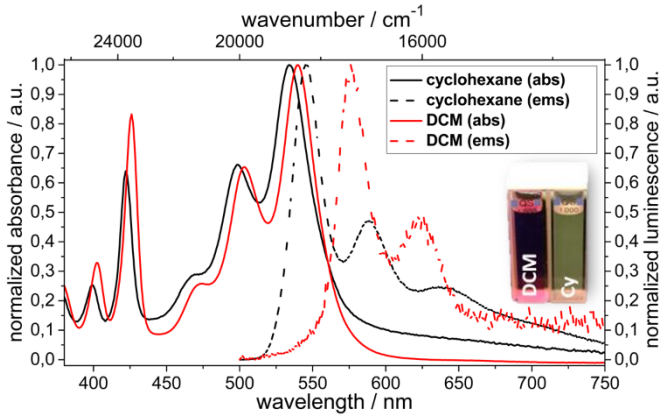


Fig. 3 Absorption und emission spectra of **TPA-BNCDI** in DCM and cyclohexane. The photograph shows **TPA-BNCDI** in DCM (left)/cyclohexane (right) under irradiation with UV-lamp at 365 nm in the dark.

Table 2 Solvent-dependent luminescence of **TPA-BNCDI** in cyclohexane and DCM.

compound	solvent	λ_{abs} / nm	λ_{ems} / nm	$\Delta\nu_{Stokes}$ /cm^{-1}	Φ_{lum} [a]
TPA-BNCDI	DCM	540	581	1307	<0.01
	cyclohexane	534	545	378	0.81

[a] Referenced externally against fluorescein in 0.1 M NaOH.

unity (Φ_{lum} = 0.95) and small Stokes shifts ($\Delta\nu_{stokes}$ = 285 - 342 cm^{-1}). Compared to all carbon **PDI** (Φ_{lum} = 0.98)[58] and **CDI** (Φ_{lum} = 0.69)[57], similar or higher quantum yields were observed.

However, the triphenylamine (TPA)-substituted **BNCDI** showed a barely visible luminescence in DCM (Table 1 and photographic image).

Variation of the aryl-substituent at the boron atom

The substitution of **BNCDI**s with strong electron-donating TPA moieties led only to a marginal bathochromic shift from 535 nm (**Tph-BNCDI**) to 541 nm (**TPA-BNCDI**) in the absorption. However, significant line broadening for the S_0-S_1 transitions (450-575 nm) and lower optical gaps (E_{opt} = 2.19 eV for **TPA-BNCDI**) compared to thienyl and phenyl-substituted **Ph/Tph-BNCDI**s (E_{opt} = 2.24-2.30 eV) were observed. A significant effect of the TPA moiety on the intensity of the high energy transitions (380-440 nm) was seen in the **TPA-BNCDI** as compared to **Ph-BNCDI** (Fig. 2). This transition (S_0-S_2) therefore involves the lateral substituents, which is a typical behavior in rylene diimides.[59, 60] In contrast to various D-A-D triads with perylene diimide as acceptor and amines as donor,[52, 53, 61, 62] the **TPA-BNCDI** absorption did not show any signature of CT character.

Although the luminescence of **TPA-BNCDI** in DCM solution was much less intense, a well-defined emission band was found with maxima at 581 nm for **TPA-BNCDI** with larger Stokes shift ($\Delta\nu_{stokes}$ = 1307 cm^{-1}) and extremely low luminescence quantum yield (Φ_{lum} = <0.01) (Fig. 3). Surprisingly, however, for solutions in nonpolar solvents (*n*pentane, *n*hexane, cyclohexane) an intense luminescence was observed for **TPA-BNCDI**. To further investigate this phenomenon, **TPA-BNCDI** were studied by UV/Vis absorption and photoluminescence spectroscopy in cyclohexane. For both the polar (DCM) and non-polar (cyclohexane) solvent, the UV-vis spectra of **TPA-BNCDI** appeared similar with a slight hypsochromic shift and slightly more marked vibronic progression in cyclohexane (Fig. 3). In contrast with the low luminescence quantum yield in DCM (Φ_{lum} = < 0.01), the **TPA-BNCDI** exhibited a strong and bright emission (λ_{ems} = 545 nm and Φ_{lum} = 0.81 for **TPA-BNCDI**) accompanied by a smaller Stokes shift in cyclohexane (378 cm^{-1}) (Fig. 3, Table 2). As phenyl- and thienyl-substituted **BNCDI**s are highly emissive in both DCM and cyclohexane, we assigned this solvent-depending quenching effect exclusively to electronic effects from the triphenylamine moiety in the **TPA-BNCDI** (see below for more details).

Electrochemical characterization

To investigate the influence of the boron substitution and the resulting photophysical properties, cyclic voltammetric measurements for all **BNCDI**s were conducted (Table 3). All measurements were performed in DCM with a three electrode configuration: working electrode (platinum disk), reference electrode (calomel electrode) and counter-electrode (platinum wire).

All **BNCDI**s exhibited two one-electron fully reversible reduction waves and either an irreversible oxidation (**Ph/Tph-BNCDI**) or fully reversible oxidation (**TPA-BNCDI**) (Fig. 4). In the case of **TPA-BNCDI**, the oxidation wave was shifted to lower potentials by 0.39 V whereas the reduction was only slightly affected by the aryl substituent at the boron atom. The onsets of the reduction indicated that the electrochemical equivalent to the LUMO[‡] ranged from E_{LUMO}(**Ph-BNCDI**) = -3.75 eV to E_{LUMO}(**Tph-BNCDI**) = -3.66 eV, and thus they were slightly more stabilized compared to **CDI** (E_{LUMO} = − 3.62 eV)[57](Table 3).

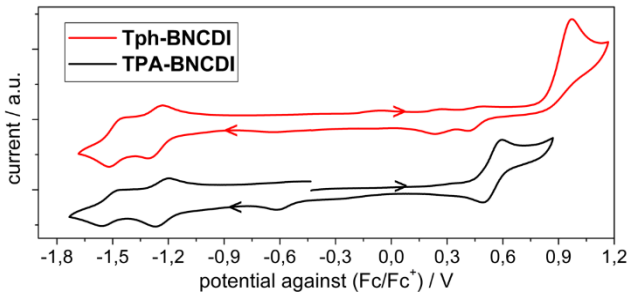
The reversible oxidation process of the **TPA-BNCDI** at +0.54 V (Fig. 4, Table 3) was also observed by spectroelectrochemical measurements, which were used to characterize its origin. It was shown that the *in situ* generated **(TPA-BNCDI)$^{\bullet+}$** and **(TPA-BNCDI)$^{2+}$** species showed red-shifted absorption ranging to the NIR region of light. Interestingly, the absorption spectra were fully regenerated to the neutral **TPA-BNCDI** (Fig. 5) upon reduction, which impressively illustrates not only the thermal but also the electrochemical stability of these BN-PAHs. Due to its redox behavior, the **TPA-BNCDI**s has a good potential to be

Table 3 Overview of electrochemical properties of all **BNCDI**s in DCM with *n*Bu$_4$NPF$_6$ (0.2 M), a scan rate of 200 mV/s and ferrocene/ferrocenium as reference.

Compound	E_{ox1} / V	E_{red1} / V	E_{red2} / V	E_{ox}^{c} / V	E_{red}^{c} / V	ΔE / V	E_{LUMO} / eV
Ph-BNCDI	+0.93[a]	-1.30[b]	-1.50[b]	0.77	-1.09	1.86	-3.71
Tph-BNCDI	+0.93[a]	-1.26[b]	-1.48[b]	0.74	-1.10	1.84	-3.66
TPA-BNCDI	+0.54[b]	-1.32[b]	-1.63[b]	0.36	-1.15	1.51	-3.69

[a] Irreversible process [b] Reversible process (ΔE_p < 60 mV) [c] E_{ox} and E_{red} represent the respective onsets. Further details in the ESI and footnote[‡].

Fig. 4 Cyclic voltammogram of **TPA-BNCDI** and **Tph-BNCDI** (10^{-3} M) in DCM with *n*Bu$_4$NPF$_6$ (10^{-2} M) as conducting salt.



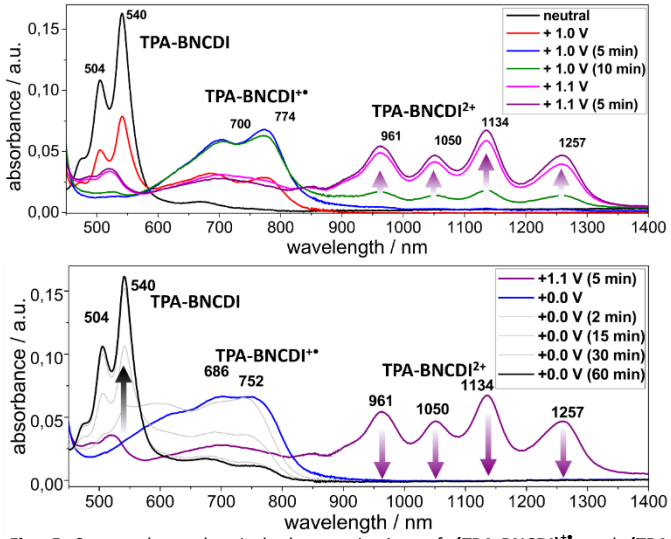


Fig. 5 Spectroelectrochemical characterization of **(TPA-BNCDI)$^{+\bullet}$** and **(TPA-BNCDI)$^{2+}$** upon oxidation (top) and the regeneration of the **TPA-BNCDI** (bottom). All experiments were performed in DCM with 0.2 M nBu$_4$NPF$_6$ at different potentials. The analyte's concentration was 10^{-4} M.

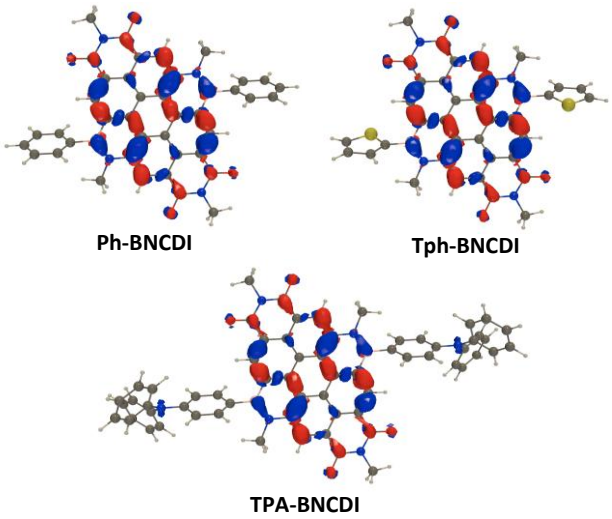


Fig. 6 Electron density difference plots for the three compounds (contour 0.001 au). Blueberry and crimson lobes correspond to density decrease and increase upon excitation. For computational reasons, the imide and alkyl functionality were simplified to a methyl group.

used in ambipolar OFET devices.[63] However, by the substitution of the **BNCDI** with TPA-groups the total electrochemical gap was reduced from $\Delta E \approx 1.85$ V for **Ph/Tph-BNCDIs** to $\Delta E \approx 1.50$ V for TPA-BNCDI (Table 3). Interestingly, the absorption spectra (Fig. 2) gave nearly identical optical gaps for the various substituents on the boron (Ph, Tph or TPA). Moreover, there is such a marked difference between the two analyses hints that the oxidation process in **TPA-BNCDI** does not involve the coronene core but is limited to the TPA-substituent.

Theoretical Calculations

To obtain more insights into the photochemical behavior of the **BNCDI**s depending on their substitution patterns, we carried out first principle calculations using a protocol described in the ESI. In these calculations, the solubilizing hexyl chains and imide groups were replaced by methyl fragments as their influence on the optical properties can be assumed to be small. In all cases, the TD-DFT calculations returned bright S_0-S_1 transitions with a clear $\pi-\pi^*$ character centered on the coronene core of the dyes. The nature of the transition can be illustrated in the form of electron density difference (EDD) plots (Fig. 6). Eminently, in all three systems, the changes of densities are centered on the core of the dye and substituents on boron had no (Ph and Th) or minor (TPA) contributions. This is in perfect agreement with the observations from the absorption spectra obtained (Fig. 2).

To perform more quantitative comparisons between experiment and theory, we have determined the 0-0 energies using hybrid CC2/TD-DFT protocols (see the ESI). These 0-0 energies can be directly compared to the crossing point between the absorption and fluorescence curves in the experimental spectra, which contrasts with the "traditional" vertical transition energies that have no clear experimental counterpart. For both the **Ph/Tph-BNCDI**s, theory returns a 0-0 wavelength of 556 nm in cyclohexane. The experimental values are close to 540 nm, which highlights the good quality of the simulation. When going to TPA, theory predicts a redshift of 44 nm leading to a 0-0 wavelength at 600 nm. Experimentally, there is also a redshift, though less pronounced with a crossing point at 545 nm (+5 nm). In any case, these limited changes are in accordance with the small extra donating character provided by the TPA groups (Fig. 6). Although such a comparison should be made with care, the vertical absorption and fluorescence were computed for the **TPA-BNCDI** in both cyclohexane and DCM yielding a solvatochromic increase of the Stokes shift by $\Delta\nu = 1015$ cm^{-1}. This was in line with the experimental value ($\Delta\nu = 929$ cm^{-1} for **TPA-BNCDI**, derived from Table 2). When comparing the S_1 (emissive) geometries of the **TPA-BNCDI** computed in cyclohexane and DCM, no obvious change appeared. Therefore, the observed increase in the Stokes shift from cyclohexane to DCM could be attributed exclusively to solvatochromic effects due to an increased CT-character.

To explain the strong solvent-depending luminescence quenching (Fig. 3, Table 2), the possibility of a photoinduced electron transfer (**PeT**) was investigated. The MO diagram (Fig. 7) shows that in the **TPA-BNCDI** the lowest energy electronic transition given by TD-DFT mainly corresponds to a HOMO-2 to LUMO excitation (74% of the total). Those two orbitals are localized in the **BNCDI** core as expected from the above analysis (Fig. 6). However, the two highest occupied MOs are nearly degenerated and clearly TPA-centred, which is a typical electronic configuration allowing **PeT** and also explaining the difference between the electrochemical and optical gaps found experimentally. In contrast to this, the **Tph-BNCDI** holds a bright transition to the lowest excited state with a clearly dominant HOMO-LUMO character (95%), preventing such **PeT** to appear. To confirm the possibility of **PeT** in **TPA-BNCDI**, we performed a constrained DFT optimization (see computational details), imposing that one electron is lost by one TPA unit and gained by the **BNCDI** core (no constraint on the second TPA). In such a way, one models the charge-separated state generated by **PeT**. We compared the energy in this constrained scenario to the one of the lowest (bright) excited-state optimized with TD-DFT. It turned out that the relaxed charge-separated structure obtained with constrained DFT is slightly more stable than the relaxed local state obtained with TD-DFT, by -0.10 eV according

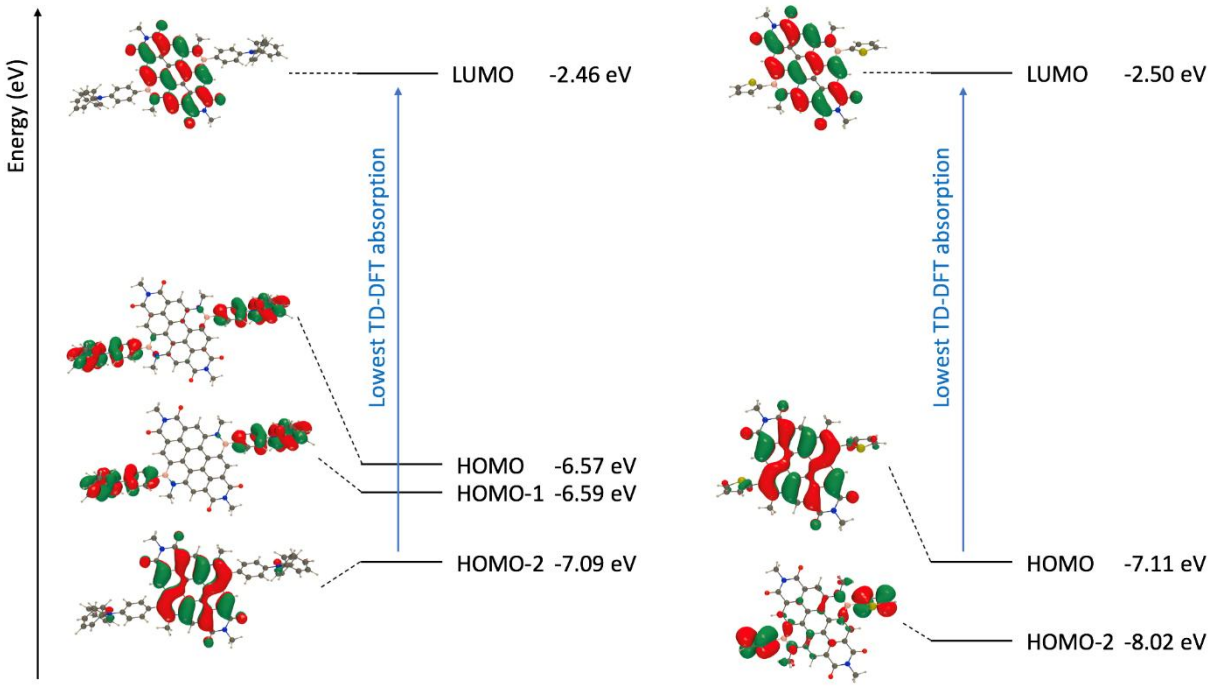


Fig. 7 MO energy diagram for the **TPA-BNCDI** (left) and **Tph-BNCDI** (right) at the PCM-CAM-B3LYP/6-31+G(d) level. The dominant character of the lowest transition corresponding to the main absorption band as modelled by PCM-TD-CAM-B3LYP/6-31+G(d) is given as well.

to this approach. Although such comparisons should always be made with care, this indicates that in DCM a **PeT** process is energetically feasible in **TPA-BNCDI**, therefore explaining the emission quenching of that system.

Moreover, as the TPA motif in **D-A-D** triads is prone to generating TICT states,[49, 64-66] we also performed relaxed TD-DFT scans of the rotational coordinates in both solvents but no evidence for this assumption was found (see the ESI).

Therefore, these findings (electrochemical analysis, solvent-dependent luminescence, and theory) all support **PeT** to be the main quenching mechanism with an electron transferred from the donor (TPA) to the excited dye (**BNCDI***).

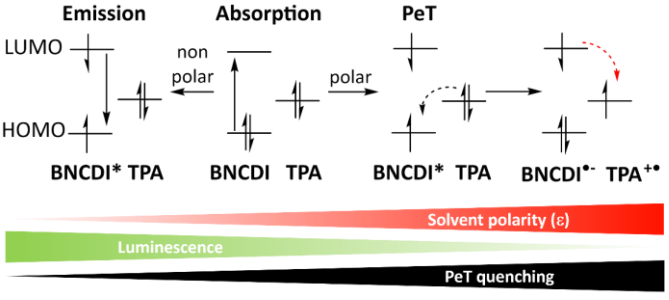
The low luminescence quantum yield in DCM correlates with a strong **PET** process whereas in a nonpolar solvent (cyclohexane), the generation of dissolved excited suppressed. To further assess the probability for a **PET**, a Rehm-Weller analysis[67-69] was performed (see the ESI). With this model, the **PeT** driving force, ΔG_{PeT}°, could be estimated to be -0.31 eV or − 6.69 kcal/mol for **TPA-BNCDI** in DCM, representing an exergonic process. On the other hand, in the non-polar cyclo-hexane the ΔG_{PeT}° was positive (0.39 eV, 8.99 kcal/mol) and therefore the **PeT** process in cyclohexane would be endergonic. This analysis explains the finding of the strong luminescence in cyclohexane and diminished luminescence in more polar DCM solutions (Scheme 1).

Lewis behavior

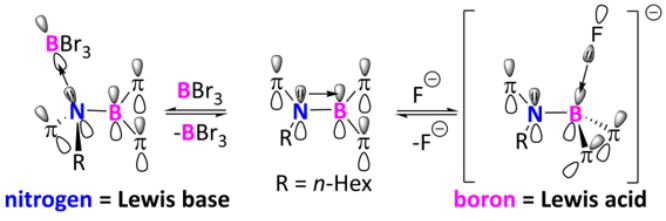
After the role of the boron substituent was assigned with the photophysical and redox properties for the **BNCDI**s, we investigated the influence of the aryl substituent on the strength of the intramolecular Lewis acid-base interaction between the nitrogen and boron atoms (Scheme 2). As we embedded the BN units at the periphery of a chromophore, we were interested in the optical response of the **BNCDIs**. Most recent examples for the interaction of BN-PAHs with Lewis acids and bases are described for fluoride ions, as Lewis base, and boron tribromide, which coordinate to the nitrogen atom, as a Lewis acid. [41, 70, 71] Therefore, we studied the interaction of the present **BNCDI**s with either fluoride or boron tribromide and measured their photophysical response.

In particular, the coordination of a fluoride anion to the boron atom should lead to a strong photophysical response as the

Scheme 1 Proposed fluorescence (non-polar solvent) and intramolecular PeT (polar solvent) mechanism for **TPA-BNCDI**.



Scheme 2 Schematic formation of different Lewis adducts and the influence on the π-conjugated scaffold. All complexes were reversible by adding a protic solvent or strong dilution.



electron-accepting boron is formally receiving two electrons. The resulting motif could yield CT-based absorption, which could not be achieved by substituting the boron atom with TPA.

Interaction with Lewis bases (F^-)

Upon the addition of an excess of tetrabutylammonium fluoride (TBAF) to DCM solutions of **TPA-BNCDI** and **Tph-BNCDI**, the color of the solution changed from red to faint green without any visible luminescence (Fig. 8).

The absorption spectra of this solution showed new absorption bands in the NIR region with peaks around 791/805 nm and a small shoulder at 709/730 nm. In the higher energy region of absorption (390 – 450 nm), two signals were detected which were assigned to be likely the S_0-S_2 transition including its vibronic fine structure. The substantial bathochromic shift of 252/262 nm compared to the free **BNCDI**s points to significant (geo)electronical changes of **BNCDI** upon fluoride addition (Scheme 2). The strong electron-donating nature of the TPA substituent at the boron atom led to a larger bathochromic shift than for the thienyl group. Titration of TBAF with **TPA-BNCDI/Tph-BNCDI** showed no additional influence of the triphenylamine on the Lewis activity. However, a two-step process with an intermediate species, indicating sequent addition to the BN units, was evidenced *via* titration experiments (ESI, Fig. S89).

Interestingly, the absorption spectra of **Tph-BNCDI** interacting with fluoride anions were similar to the absorption spectra of **Tph-BNCDI** radical anion and dianion species (Fig. S85) implying a similar spatial arrangement and energetic distribution of the reduced species' frontier orbitals.

Due to the strong bathochromic shift of **TPA-BNCDI** and **Tph-BNCDI** in combination with a fluoride source, we were interested to know if the resulting adduct complexes exhibit fluorescence quenching as reported previously for several highly polar Lewis acid/base adduct systems.[41] In contrast to these earlier reports, we observed strong emission bands in the UV/Vis region (380-600 nm) and the NIR region (700-950 nm) without any vibrational fine structure (Fig. 10). Furthermore, relatively small Stokes shifts (737 cm^{-1} for **TPA-BNCDI**, 692 cm^{-1} for **Tph-BNCDI**) were observed.

Surprisingly, all **BNCDI**s also exhibited interaction with weaker Lewis bases (THF, ethyl acetate, triethylamine, acetonitrile) resulting in drastic changes of the absorption spectra but conserving the typical vibronic signatures of the absorption bands (Fig. S92/S93 in the ESI).

Interaction with Lewis acids (BBr_3)

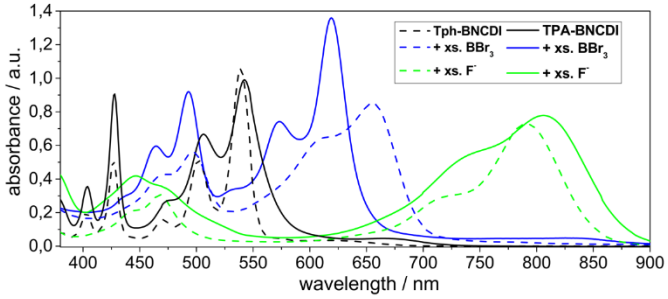
The addition of **BBr_3** to **TPA-BNCDI** and **Tph-BNCDI** led to the formation of a blue species with red-shifted absorption maxima (619/656 nm) and shoulder peaks (573/608 nm), again displaying a vibronic fine structure (Fig. 9). In the higher energy absorbing region, two new signals (493/497 nm, 464/468 nm) were found with a similar vibronic topology. Besides the bathochromic shift (37 nm) of **TPA-BNCDI** compared to **Tph-BNCDI**, an additional Lewis activity of the nitrogen lone pair of the triphenylamine was not found via titration experiments. Here a two-step process with clearly distinguished intermediates was evidenced again (ESI, Fig. S91).

Generally, the fluoride **BNCDI** species could be transformed to the **BBr_3 BNCDI** but not *vice versa* suggesting that the **BBr_3 BNCDI** had superior stability. However, all Lewis acid/base adducts species could be readily reversed by the addition of protic solvents to restore the respective **BNCDI**s.

Fig. 8 This photographic image is showing solutions of **Tph-BNCDI** in DCM, with BBr_3 and with TBAF (from left to right) as well as **TPA-BNCDI** in DCM, with BBr_3 and with TBAF (from left to right).



Fig. 9 Absorption spectra of **TPA-BNCDI/Tph-BNCDI** and their interaction with BBr_3 and TBAF.



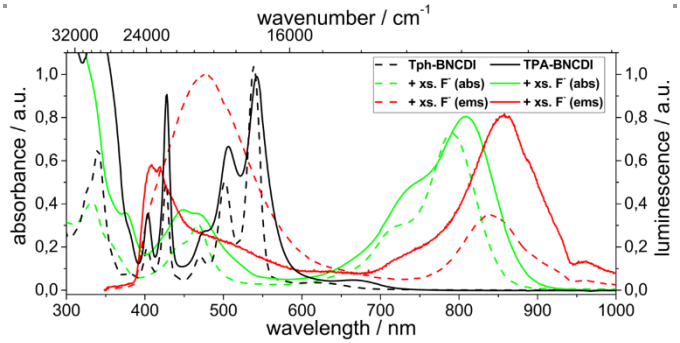


Fig. 10 Absorption and emission spectra (excited at 375 nm), of **Tph-BNCDI** and of **TPA-BNCDI** with an excess of TBAF in DCM.

Conclusions

A family of phenyl-, thienyl- and triphenylamine-substituted **BNCDI**s representing the first BN-based **D-A-D** triads were prepared and fully characterized. Using this novel motif, we could show and explain how and why the substituents on the boron/nitrogen unit affect the photophysical properties of a BN-PAHs. In contrast to its CC-analogs, the effect of the donor group on the absorption was rather minor and the lowest absorption band did not show any significant charge-transfer character. However, we observed a solvent-dependent luminescence quenching process for the triphenylamine motif. The strong solvent-tunable luminescence for **TPA-BNCDI** (Φ_{lum} (DCM) < 0.01, Φ_{lum}(cyclohexane) = 0.81) and the lower oxidation potential for the **TPA-BNCDI** suggested an intramolecular photoinduced electron transfer (**PeT**) quenching process which was confirmed by both C-DFT/TD-

DFT analysis and the Rehm-Weller analyses. Moreover, this study shed light on the substitutional effect on the boron/nitrogen atoms as the Lewis behavior of the BN unit was directly influenced. Those results impact the general understanding of BN-PAH and the role of the substituents on the boron/nitrogen atoms. Strikingly, the electron-rich triphenylamine-substituents led to a stronger red-shift of the absorption band but a more intense blue-shift for coordination by a Lewis acid. Due to beneficial photophysical properties, their high thermal and electronic stability, the performance of the **BNCDI**s will be evaluated soon in organic devices (OLED, OFET). In particular, the **TPA-BNCDI** hold potential for ambipolar OFETs and two-photon absorption materials. Moreover, PeT-active materials like the **TPA-BNCDI** are widely used as photocatalyst.[72] In our case, also the sensitivity to the permittivity of the given environment (cyclohexane vs. DCM) and the respective dependency of the luminescence intensity could be useful to determine the polarity in various cellular compartments using luminescence bioimaging (e.g. FLIM).

Conflicts of interest

There are no conflicts to declare.

Acknowledgements

J.H. and A.S. acknowledge funding from the DFG (Emmy-Noether fellowship for A.S.)(STA1195/2-1). We also thank Prof. Dr. Frank Sönnichsen (University of Kiel, Germany) for conducting the ^{11}B NMR experiments. Y. Molard and G. Taupier (Scanmat-UMS 2001) are thanked for NIR emission measurements. This work is supported by the Ministère de la Recherche et de l'Enseignement Superieur, the CNRS, the Region Bretagne, and COST CM 1302 (SIPS). This work used the computational resources of the CCIPL center installed in Nantes, France.

References

1. C. Aumaitre, J. F. Morin, *Chem. Rec.*, **2019**, *19*, 1142-1154.
2. Z. Liu, Y. Wu, Q. Zhang, X. Gao, *J. Mater. Chem. A*, **2016**, *4*, 17604-17622.
3. J. Mei, Y. Diao, A. L. Appleton, L. Fang, Z. Bao, *J. Am. Chem. Soc.*, **2013**, *135*, 6724-6746.
4. M. Stepien, E. Gonka, M. Zyla, N. Sprutta, *Chem. Rev.*, **2017**, *117*, 3479-3716.
5. C. Wang, H. Dong, W. Hu, Y. Liu, D. Zhu, *Chem. Rev.*, **2012**, *112*, 2208-2267.
6. J. E. Anthony, *Chem. Rev.*, **2006**, *106*, 5028-5048.
7. J. Wu, W. Pisula, K. Müllen, *Chem. Rev.*, **2007**, *107*, 718-747.
8. A. Narita, X. Y. Wang, X. Feng, K. Müllen, *Chem. Soc. Rev.*, **2015**, *44*, 6616-6643.
9. L. Schmidt-Mende, A. Fechtenkotter, K. Müllen, E. Moons, R. H. Friend, J. D. MacKenzie, *Science*, **2001**, *293*, 1119-1122.
10. L. Chen, C. Li, K. Müllen, *J. Mater. Chem. C*, **2014**, *2*, 1938-1956.
11. F. Würthner, C. R. Saha-Möller, B. Fimmel, S. Ogi, P. Leowanawat, D. Schmidt, *Chem. Rev.*, **2015**, *116*, 962-1052.
12. T. Weil, T. Vosch, J. Hofkens, K. Peneva, K. Müllen, *Angew. Chem. Int. Ed.*, **2010**, *49*, 9068-9093.
13. Z. Zhao, Z. Yin, H. Chen, L. Zheng, C. Zhu, L. Zhang, S. Tan, H. Wang, Y. Guo, Q. Tang, Y. Liu, *Adv. Mater.*, **2017**, *29,* 1602410.
14. P. Osswald, D. Leusser, D. Stalke, F. Würthner, *Angew. Chem. Int. Ed.*, **2004**, *44*, 250-253.
15. G. Li, D. Li, X. Liu, H. Xu, J. Zhang, S. Wang, Z. Liu, B. Tang, *Chem. Commun.*, **2019**, *55*, 9661-9664.
16. D. Sun, D. Meng, Y. Cai, B. Fan, Y. Li, W. Jiang, L. Huo, Y. Sun, Z. Wang, *J. Am. Chem. Soc.*, **2015**, *137*, 11156-11162.
17. Y. Zhou, B. Xue, C. Wu, S. Chen, H. Liu, T. Jiu, Z. Li, Y. Zhao, *Chem. Commun.*, **2019**, *55*, 13570-13573.
18. A. D. Hendsbee, J.-P. Sun, W. K. Law, H. Yan, I. G. Hill, D. M. Spasyuk, G. C. Welch, *Chem. Mater.*, **2016**, *28*, 7098-7109.
19. F. You, X. Zhou, H. Huang, Y. Liu, S. Liu, J. Shao, B. Zhao, T. Qin, W. Huang, *New J. Chem.*, **2018**, *42*, 15079-15087.
20. Z. Liu, T. B. Marder, *Angew. Chem. Int. Ed.*, **2008**, *47*, 242-244.
21. M. M. Morgan, W. E. Piers, *Dalton Trans.*, **2016**, *45*, 5920-5924.
22. M. J. D. Bosdet, W. E. Piers, *Can. J. Chem.*, **2009**, *87*, 8-29.
23. P. G. Campbell, A. J. Marwitz, S. Y. Liu, *Angew. Chem. Int. Ed.*, **2012**, *51*, 6074-6092.
24. J.-Y. Wang, J. Pei, *Chin. Chem. Lett.*, **2016**, *27*, 1139-1146.
25. T. Hatakeyama, S. Hashimoto, S. Seki, M. Nakamura, *J. Am. Chem. Soc.*, **2011**, *133*, 18614-18617.
26. J. Huang, Y. Li, *Front. Chem.*, **2018**, *6*, 341.
27. T. Hatakeyama, S. Hashimoto, S. Seki, M. Nakamura, *J. Am. Chem. Soc.*, **2011**, *133*, 18614-18617.
28. S. R. Wisniewski, C. L. Guenther, O. A. Argintaru, G. A. Molander, *J. Org. Chem.*, **2014**, *79*, 365-378.
29. C. Zhang, L. Zhang, C. Sun, W. Sun, X. Liu, *Org. Lett.*, **2019**, *21*, 3476-3480.
30. M. J. S. Dewar, V. P. Kubba, R. Pettit, *J. Chem. Soc.*, **1958**, 3073-3076.
31. M. J. Bosdet, C. A. Jaska, W. E. Piers, T. S. Sorensen, M. Parvez, *Org. Lett.*, **2007**, *9*, 1395-1398.
32. M. J. Bosdet, W. E. Piers, T. S. Sorensen, M. Parvez, *Angew. Chem. Int. Ed.*, **2007**, *46*, 4940-4943.
33. Y. Appiarius, T. Stauch, E. Lork, P. Rusch, N. C. Bigall, A. Staubitz, *Org. Chem. Front.*, **2020**.
34. T. Kaehler, M. Bolte, H.-W. Lerner, M. Wagner, *Angew. Chem. Int. Ed.*, **2019**, *58*, 11379-11384.
35. A. Abengozar, P. Garcia-Garcia, D. Sucunza, A. Perez-Redondo, J. J. Vaquero, *Chem. Commun.*, **2018**, *54*, 2467-2470.
36. X. Fang, H. Yang, J. W. Kampf, M. M. Banaszak Holl, A. J. Ashe, *Organometallics*, **2006**, *25*, 513-518.
37. A. J. Ashe, X. Fang, *Org. Lett.*, **2000**, *2*, 2089-2091.
38. P. B. Pati, E. Jin, Y. Kim, Y. Kim, J. Mun, S. J. Kim, S. J. Kang, W. Choe, G. Lee, H. J. Shin, Y. S. Park, *Angew. Chem. Int. Ed.*, **2020**, *59*, 14891-14895.
39. S. Wang, D. T. Yang, J. Lu, H. Shimogawa, S. Gong, X. Wang, S. K. Mellerup, A. Wakamiya, Y. L. Chang, C. Yang, Z. H. Lu, *Angew. Chem. Int. Ed.*, **2015**, *54*, 15074-15078.
40. F. D. Zhuang, Z. H. Sun, Z. F. Yao, Q. R. Chen, Z. Huang, J. H. Yang, J. Y. Wang, J. Pei, *Angew. Chem. Int. Ed.*, **2019**, *58*, 10708-10712.

41. G. Li, Y. Zhao, J. Li, J. Cao, J. Zhu, X. W. Sun, Q. Zhang, *J. Org. Chem.*, **2015**, *80*, 196-203.
42. S. Horiuchi, T. Hasegawa, Y. Tokura, *J. Phys. Soc. Jpn.*, **2006**, *75*, 051016.
43. X. Wan, C. Li, M. Zhang, Y. Chen, *Chem. Soc. Rev.*, **2020**, *49*, 2828-2842.
44. J. Song, K. Zhao, H. Zhang, C.-K. Wang, *Mol. Phys.*, **2018**, *117*, 672-680.
45. R. Sen, S. P. Singh, P. Johari, *J. Phys. Chem. A*, **2018**, *122*, 492-504.
46. K. Zhou, H. Dong, H. L. Zhang, W. Hu, *Phys. Chem. Chem. Phys.*, **2014**, *16*, 22448-22457.
47. A. Leliege, P. Blanchard, T. Rousseau, J. Roncali, *Org. Lett.*, **2011**, *13*, 3098-3101.
48. Y. Sun, G. C. Welch, W. L. Leong, C. J. Takacs, G. C. Bazan, A. J. Heeger, *Nat. Mater.*, **2011**, *11*, 44-48.
49. R. Misra, S. P. Bhattacharyya, *Intramolecular Charge Transfer: Theory and Applications*, Wiley VCH, Weinheim, **2018**.
50. Y. Shibano, H. Imahori, C. Adachi, *Journal of Physical Chemistry C*, **2009**, *113*, 15454-15466.
51. S. Vajiravelu, L. Ramunas, G. Juozas Vidas, G. Valentas, J. Vygintas, S. Valiyaveettil, *J. Mater. Chem.*, **2009**, *19*, 4268.
52. L. Cao, L. Xu, D. Zhang, Y. Zhou, Y. Zheng, Q. Fu, X.-F. Jiang, F. Lu, *Chem. Phys. Lett.*, **2017**, *682*, 133-139.
53. Y. Shibano, H. Imahori, C. Adachi, *J. Phys. Chem. C*, **2009**, *113*, 15454-15466.
54. R. Mishra, J. M. Lim, M. Son, P. Panini, D. Kim, J. Sankar, *Chemistry*, **2014**, *20*, 5776-5786.
55. E. Fron, R. Pilot, G. Schweitzer, J. Qu, A. Herrmann, K. Müllen, J. Hofkens, M. Van der Auweraer, F. C. De Schryver, *Photochem. Photobiol. Sci.*, **2008**, *7*, 597-604.
56. S. A. Iqbal, J. Pahl, K. Yuan, M. J. Ingleson, *Chem. Soc. Rev.*, **2020**.
57. C. L. Eversloh, C. Li, K. Müllen, *Org. Lett.*, **2011**, *13*, 4148-4150.
58. A. Rademacher, S. Märkle, H. Langhals, *Chem. Ber.*, **1982**, *115*, 2927-2934.
59. J. Calbo, A. Doncel-Giménez, J. Aragó, E. Ortí, *Theor. Chem. Acc.*, **2018**, *137*.
60. Y. Avlasevich, C. Li, K. Müllen, *J. Mater. Chem.*, **2010**, *20*, 3814.
61. M. Kojima, A. Tamoto, N. Aratani, H. Yamada, *Chem. Commun.*, **2017**, *53*, 5698-5701.
62. C. C. Chao, M. K. Leung, Y. O. Su, K. Y. Chiu, T. H. Lin, S. J. Shieh, S. C. Lin, *J. Org. Chem.*, **2005**, *70*, 4323-4331.
63. C. Rost, D. J. Gundlach, S. Karg, W. Rieß, *J. Appl. Phys.*, **2004**, *95*, 5782-5787.
64. Z. R. Grabowski, K. Rotkiewicz, W. Rettig, *Chem. Rev.*, **2003**, *103*, 3899-4032.
65. S. Sasaki, G. P. C. Drummen, G.-i. Konishi, *J. Mater. Chem. C*, **2016**, *4*, 2731-2743.
66. H. Li, J. Han, H. Zhao, X. Liu, Y. Luo, Y. Shi, C. Liu, M. Jin, D. Ding, *J. Phys. Chem. Lett.*, **2019**, *10*, 748-753.
67. D. Rehm, A. Weller, *Z. Phys. Chem.*, **1970**, *69*, 183-200.
68. J. R. Lakowicz, *Principles of Fluorescence Spectroscopy*, Springer US, Boston, 3rd edn., **2006**.
69. A. Nowak-Krol, B. Fimmel, M. Son, D. Kim, F. Würthner, *Faraday Discuss.*, **2015**, *185*, 507-527.
70. Y. Chen, W. Chen, Y. Qiao, G. Zhou, *Chemistry*, **2019**, *25*, 9326-9338.
71. M. Lepeltier, O. Lukoyanova, A. Jacobson, S. Jeeva, D. F. Perepichka, *Chem. Commun.*, **2010**, *46*, 7007-7009.
72. A. G. Griesbeck, N. Hoffmann, K. D. Warzecha, *Acc. Chem. Res.*, **2007**, *40*, 128-140.

Footnote

† Electronic supplementary information (ESI) available. See DOI: 10.1039/x0xx00000x

‡ Although this is often referred to as the LUMO, and Table 3 is resented as E_{LUMO}, we wish to point out that actually the LUMO cannot be measured in this way, as it is not defined electrochemically.